International Journal of Modern Physics E
© World Scientific Publishing Company

arXiv:1409.4645v2 [nucl-th] 5 Dec 2014

# Shape co-existence and parity doublet in Zr isotopes

Bharat Kumar*, S. K. Singh, S. K. Patra
*Institute of Physics, Bhubaneswar-751 005, India.*

Received (received date)
Revised (revised date)
Accepted (Day Month Year)

We studied the ground and excited states properties for Zr isotopes starting from proton to neutron drip-lines using the relativistic and non-relativistic mean field formalisms with BCS and Bogoliubov pairing. The celebrity NL3 and SLy4 parameter sets are used in the calculations. We find spherical ground and low-lying largedeformed excited states in most of the isotopes. Several couples of $\Omega^{\pi} = 1/2^{\pm}$ parity doublets configurations are found, while analyzing the single-particle energy levels of the largedeformed configurations.

*Keywords*: Relativistic mean field theory, Skyrme Hartree-Fock-Bogoliubov theory, Parity doublet, Shape co-existence

PACS Number(s): 21.10.Dr,21.10.Hw,21.10.Ft,21.10.Pc

## 1. Introduction

Although the nuclear shape co-existence for various mass regions of the periodic table is a well known phenomena, it remains an interesting investigation till today. On the other hand, the existence of parity doublet is relatively new.[1,2] The origin and manifestation of such an interesting observable is not yet known clearly. It is reported that the parity doublet is not visible in a nucleus with normal/spherical deformation. However, the existence of parity doublet is possible for nuclei with highly deformed shape. In this case, two orbitals with opposite parity lie very close to each other. Since, the parity doublet is only appeared in largedeformed configuration and not in normal or spherical shape, the possibility of its origin may be related to its shape, i.e. with deformed orbitals. That means, in normal situation, the high lying partner of the doublet does not come nearer to the low lying one but when the nucleus gets deformed, gives rise a Nilsson like structure in the largedeformed state. The shape co-existence, i.e., two different shapes with very close in energy is also a rare, but known incident in nuclear structure physics.[3–7] In this case, both the solutions are nearly or completely degenerate (different configuration with same energy). This phenomenon is mostly visible in the mass region $A = 100$

*Email: bharat@iopb.res.in

of the periodic table.[8] Here, we have chosen Zr nucleus as a potential candidate both for shape co-existence and study of parity doublets using the well known relativistic (RMF) and non-relativistic (SHF) mean field formalisms. The NL3 and SLy4 parametrization with BCS and Bogoliubov pair prescriptions used to take care of the pairing for the open shell nuclei.

The paper is organized as follows: In sections 2 and 3, we have given a brief outline about the non-relativistic Skyrme-Hartree-Fock-Bogoliubov (SHFB) and relativistic mean field (RMF) formalisms. Our results are discussed in section 4. A concluding remark is given in section 5.

## 2. Skyrme-Hartree-Fock-Bogoliubov Approximation :

The energy density functional with Skyrme-Hartree-Fock-Bogoliubov Approximation is a powerful theoretical formalism to deal with finite nuclei starting from both proton to neutron drip-lines.[9] In this calculations, we have used the most successful SLy4 parameter set[10] with zero-range Bogoliubov pairing interaction for open shell nuclei. The numerical calculations are done using an axially deformed Harmonic oscillator (HO) basis state expansion to solve the Schrödinger equation iteratively. The numerical calculations are carried out using the code HFBTHO (v1.66p)[11] that solve the equation self-consistently. For Skyrme forces, the HFB energy has the form of a local energy density functional:[14–17]

$$E[\rho,\tilde{\rho}] = \int d^3\mathbf{r}\ \mathcal{H}(\mathbf{r}), \tag{1}$$

where, Hamiltonian density $\mathcal{H}$:

$$\mathcal{H}(\mathbf{r}) = H(\mathbf{r}) + \tilde{H}(\mathbf{r}) \tag{2}$$

is the sum of the mean-field and pairing energy densities. In the present implementation, we use the following explicit forms:

$$\begin{aligned} H(\mathbf{r}) = {} & \tfrac{\hbar^2}{2m}\tau + \tfrac{1}{2}t_0\left[\ \left(1+\tfrac{1}{2}x_0\right)\rho^2 - \left(\tfrac{1}{2}+\ x_0\right)\sum_q \rho_q^2\ \right] \\ & + \tfrac{1}{2}t_1\left[\ \left(1+\tfrac{1}{2}x_1\right)\rho\left(\tau-\tfrac{3}{4}\ \Delta\rho\right)\right] - \left(\tfrac{1}{2}+\ x_1\right)\sum_q \rho_q\left(\tau_q-\tfrac{3}{4}\Delta\rho_q\right)\Big] \\ & + \tfrac{1}{2}t_2\left[\ \left(1+\tfrac{1}{2}x_2\right)\rho\left(\tau+\tfrac{1}{4}\Delta\rho\right) - \left(\tfrac{1}{2}+\ x_2\right)\sum_q \rho_q\left(\tau_q+\tfrac{1}{4}\Delta\rho_q\right)\right] \\ & + \tfrac{1}{12}t_3\rho^\alpha\left[\left(1+\tfrac{1}{2}x_3\right)\rho^2 - \left(x_3+\tfrac{1}{2}\right)\sum_q \rho_q^2\right] \\ & - \tfrac{1}{8}\left(t_1x_1+t_2x_2\right)\sum_{ij}\mathbf{J}_{ij}^2 + \tfrac{1}{8}\left(t_1-t_2\right)\sum_{q,ij}\mathbf{J}_{q,ij}^2 \\ & - \tfrac{1}{2}W_0\sum_{ijk}\varepsilon_{ijk}\left[\rho\nabla_k\mathbf{J}_{ij} + \sum_q \rho_q\nabla_k\mathbf{J}_{q,ij}\right], \end{aligned} \tag{3}$$

$$\tilde{H}(\mathbf{r}) = \tfrac{1}{2}V_0\left[1 - V_1\left(\frac{\rho}{\rho_0}\right)^\gamma\ \right]\sum_q \tilde{\rho}_q^2. \tag{4}$$

The index $q$ labels the neutron ($q=n$) or proton ($q=p$) densities, while densities without index $q$ denote the sums of proton and neutron densities. $H(\mathbf{r})$ and $\tilde{H}(\mathbf{r})$

depend on the particle local density $\rho(\mathbf{r})$, pairing local density $\tilde{\rho}(\mathbf{r})$, kinetic energy density $\tau(\mathbf{r})$, and spin-current density $\mathbf{J}_{ij}(\mathbf{r})$. The number of oscillator shells $N_{sh} = 20$ to avoid the convergence problem and basis parameter $b_0 = \sqrt{b_z^2 + b_\perp^2}$ are used in the calculations. A detail numerical technique is available in Ref.[11] and the notations are their usual meaning.

### 2.1. *Pairing Correlations in SHF formalism*

In non-relativistic Skyrme-Hartree-Fock-Bogoliubov (SHFB) formalism, we have included pairing correlation by using Lipkin-Nogami (LN) prescription.[11,12] In this calculation, the LN method is implemented by perturbing the SHFB calculation with an additional term $h^{'} = h - 2\lambda_2(1-2\rho)$ is included in the HF Hamiltonian, where the parameter $\lambda_2$ is iteratively calculated so as to properly describe the curvature of the total energy as a function of the particle number. For an arbitrary two-body interaction $\hat{V}$, $\lambda_2$ can be calculated from the particle number dispersion according the following relation:[11]

$$\lambda_2 = \frac{< 0|\hat{V}|4 >< 4|\hat{N}^2|0 >}{< 0|\hat{N}^2|4 >< 4|\hat{N}^2|0 >}, \tag{5}$$

where $|0>$ is the quasiparticle vacuum, $\hat{N}$ is the particle number operator, and $|4 >< 4|$ is the projection operator onto the 4-quasiparticle operator space. The final expression for the $\lambda_2$ can be written in following simple form:[13]

$$\lambda_2 = \frac{1}{2}\frac{\mathrm{Tr}\Gamma'\rho(1-\rho) + \mathrm{Tr}\Delta'(1-\rho)\kappa}{[\mathrm{Tr}\rho(1-\rho)]^2 - 2\mathrm{Tr}\rho^2(1-\rho)^2}, \tag{6}$$

where $\kappa$ is the pairing tensor and potentials are given as:

$$\Gamma'_{\alpha\alpha'} = \sum_{\beta\beta'} V_{\alpha\beta\alpha'\beta'}(\rho(1-\rho))_{\beta'\beta}, \tag{7}$$

and

$$\Delta'_{\alpha\beta} = \frac{1}{2}\sum_{\alpha'\beta'} V_{\alpha\beta\alpha'\beta'}(\rho\kappa)_{\alpha'\beta'}, \tag{8}$$

which can be calculated in a full analogy to $\Gamma$ and $\Delta$ by replacing $\rho$ and $\kappa$ by $\rho(1-\rho)$ and $\rho\kappa$, respectively. In case of the seniority-pairing interaction with strength $G$, equation (6) can be simplified to

$$\lambda_2 = \frac{G}{4}\frac{\mathrm{Tr}(1-\rho)\kappa\ \mathrm{Tr}\rho\kappa - 2\ \mathrm{Tr}(1-\rho)^2\rho^2}{[\mathrm{Tr}\rho(1-\rho)]^2 - 2\ \mathrm{Tr}\rho^2(1-\rho)^2}. \tag{9}$$

The equation (6) can be well approximated by the seniority-pairing expression (9) with the effective strength (G) and can be written in terms of pairing energy ($E_{\mathrm{pair}}$) and average pairing gap ($\bar{\Delta}$):[11]

$$G = G_{\mathrm{eff}} = -\frac{\bar{\Delta}^2}{E_{\mathrm{pair}}} \tag{10}$$

where, $E_{\rm pair} = -\frac{1}{2}{\rm Tr}\Delta\kappa$ and $\bar{\Delta} = \frac{{\rm Tr}\Delta\rho}{{\rm Tr}\rho}$.

Here, calculations have done using the density dependent delta pairing force with the pairing strength $V_0$ = -244.72 MeV $fm^3$, pairing cut-off energy 60.0 MeV and pairing window 60.0 MeV. These quantities have been fitted to reproduce the neutron pairing gap of $^{120}$Sn which is consistent with Ref.[18] Average pairing gap ($\bar{\Delta}$) is obtained from the level density. Thus, it varies from nucleus to nucleus depending on the density distribution of nucleons. The results for pairing gap ($\triangle_n$, $\triangle_p$), effective strength ($G_n$, $G_p$) and pairing energy ($E_{pair}$) for Zr isotopes are given in Table 3.

## 3. Theoretical Framework for Relativistic Mean Field Model

The relativistic mean field (RMF) model[19–25] is very successful in recent years for both finite nuclei and infinite nuclear matter from normal to super-normal conditions. In the present calculations, we have used the RMF Lagrangian[19] with the NL3 parameter set,[26] which is quite successful for both $\beta$-stable and drip-lines nuclei. The Lagrangian contains the terms of interaction between mesons and nucleons and also self-interaction of isoscalar scalar *sigma* meson. The other mesons are isoscalar vector *omega* and isovector vector *rho* mesons. The photon field $A_\mu$ is included to take care of the Coulombic interaction of protons. A definite set of coupled equations are obtained from the Lagrangian which are solved self-consistently in an axially deformed Harmonic Oscillator (HO) basis with $N_F = N_B = 12$, Fermionic and Bosonic oscillator quanta, respectively. A detail study about choosing the HO basis is given in subsection 3.2. The relativistic Lagrangian density for a nucleon-meson many-body systems is written as:

$$\begin{aligned}\mathcal{L} = {} & \overline{\psi_i}\{i\gamma^\mu\partial_\mu - M\}\psi_i + \frac{1}{2}\partial^\mu\sigma\partial_\mu\sigma - \frac{1}{2}m_\sigma^2\sigma^2 - \frac{1}{3}g_2\sigma^3 - \frac{1}{4}g_3\sigma^4 - g_s\overline{\psi_i}\psi_i\sigma \\ & -\frac{1}{4}\Omega^{\mu\nu}\Omega_{\mu\nu} + \frac{1}{2}m_w^2V^\mu V_\mu - g_w\overline{\psi}_i\gamma^\mu\psi_iV_\mu - \frac{1}{4}\vec{B}^{\mu\nu}.\vec{B}_{\mu\nu} + \frac{1}{2}m_\rho^2\vec{R}^\mu.\vec{R}_\mu \\ & -g_\rho\overline{\psi}_i\gamma^\mu\vec{\tau}\psi_i.\vec{R}^\mu - \frac{1}{4}F^{\mu\nu}F_{\mu\nu} - e\overline{\psi}_i\gamma^\mu\frac{(1-\tau_{3i})}{2}\psi_iA_\mu. \end{aligned} \tag{11}$$

Here, sigma meson field is denoted by $\sigma$, omega meson field by $V_\mu$ and rho meson field by $\vec{R}_u$ and $A_\mu$ denotes the electromagnetic field, which couples to the protons. The Dirac spinors are given by $\psi$ for the nucleons, whose third component of isospin is denoted by $\tau_3$ and $g_s$, $g_2$, $g_3$, $g_\omega$, $g_\rho$ are the coupling constants. The center of mass (c.m.) motion energy correction is estimated by the harmonic oscillator approximation $E_{c.m.} = \frac{3}{4}(41A^{-1/3})$. From the resulting proton and neutron quadrupole moments, the quadrupole deformation parameter $\beta_2$ is defined as:

$$Q = Q_n + Q_p = \sqrt{\frac{16\pi}{5}}\left(\frac{3}{4\pi}AR_0^2\beta_2\right), \tag{12}$$

with $R_0 = 1.2A^{1/3}$ (fm), and the root mean square matter radius are given as:

$$\langle r_m^2\rangle = \frac{1}{A}\int\rho(r_\perp, z)r^2d\tau, \tag{13}$$

where $A$ is the mass number, and $\rho(r_\perp, z)$ is the deformed density. The total binding energy and other observables are also obtained by using the standard relations.[19,20]

### 3.1. *Pairing Correlations in RMF formalism*

The pairing correlation plays an important role in open shell nuclei to describe the ground state properties, like binding energy, charge radius, single particle energy level and deformation. The relativistic Lagrangian contains only terms like $\psi^\dagger\psi$, and no terms of the form $\psi^\dagger\psi^\dagger$ at the mean level. The inclusion of the pairing correlation of the form $\psi\psi$ and two-body interaction $\psi^\dagger\psi^\dagger\psi\psi$ in the Lagrangian violate the particle number conservation.[28] We used the pairing correlation externally in the RMF model. In our calculation, the constant gap BCS-approach take care the pairing correlation for open shell nuclei. The general expression for pairing energy in terms of occupation probabilities $v_i^2$ and $u_i^2 = 1 - v_i^2$ is written as:[28,29]

$$E_{pair} = -G\left[\sum_{i>0} u_i v_i\right]^2, \tag{14}$$

with $G$ = pairing force constant. The variational approach with respect to $v_i^2$ gives the BCS equation:[29]

$$2\epsilon_i u_i v_i - \triangle(u_i^2 - v_i^2) = 0, \tag{15}$$

using $\triangle = G\sum_{i>0} u_i v_i$.

The occupation number is defined as:

$$n_i = v_i^2 = \frac{1}{2}\left[1 - \frac{\epsilon_i - \lambda}{\sqrt{(\epsilon_i - \lambda)^2 + \triangle^2}}\right]. \tag{16}$$

The values of $\triangle$ for the nucleons (neutron and proton) is taken from the phenomenological formulae of Madland and Nix:[27]

$$\triangle_n = \frac{r}{N^{1/3}} exp(-sI - tI^2), \qquad \triangle_p = \frac{r}{Z^{1/3}} exp(sI - tI^2), \tag{17}$$

where, $I = (N - Z)/A$, $r = 5.73$ MeV, $s = 0.117$, and $t = 7.96$.

The chemical potentials $\lambda_n$ and $\lambda_p$ are determined by the particle numbers for neutrons and protons. Finally, the pairing energy is computed as:

$$E_{pair} = -\triangle \sum_{i>0} u_i v_i. \tag{18}$$

For a particular value of $\triangle$ and $G$, the pairing energy $E_{pair}$ diverges, if it is extended to an infinite configuration space. In fact, in all realistic calculations with finite range forces, the contribution of states of large momenta above the Fermi surface (for a particular nucleus) to $\triangle$ decreases with energy. Therefore, we use a pairing window, where the equations are extended up to the level $|\epsilon_i - \lambda| \leq 2(41A^{-1/3})$ which is the function of single particle energy. The factor 2 has been determined so as to reproduce the pairing correlation energy for neutrons in $^{118}$Sn using Gogny

force.[22,28,30] It is to be noted that recently Karatzikos et al.[31] has shown that if one use the constant pairing window which is adjusted for one state at particular deformation then it may lead to errors at different energy solution (different state solution). However, we have not taken this problem into account in our calculations, as we have adjusted to reproduce the pairing as a whole of $^{118}Sn$ nucleus.

### 3.2. *Selection of Basis Space*

After getting the self-consistent mean field equations for both Fermions and Bosons, we need to solve these equations by expanding the wave functions (potentials) in the deformed harmonic oscillator basis and solve the self consistent equations iteratively. For the exotic (drip-line) nuclei more harmonic oscillator quanta require to get the proper convergence of the system. In our calculations, we used the harmonic oscillator quanta $N_F$=$N_B$=12, where $N_F$ for Fermionic and $N_B$ for Bosonic quanta. The convergence of the physical observable like binding energy (BE), root mean square matter radius ($r_{rms}$) and quadrupole deformation parameter ($\beta_2$) with the harmonic oscillator basis are tested and obtained results are shown in Figure 1. We used the non-constraint calculation (free solution) to get the physical observables and for the large initial deformation basis parameter ($\beta_0 = 0.6$), because we want to check the convergence for the large deformation basis parameter. If we increase the basis quanta from 12 to 14 the increment in the energy is $\sim 0.21$MeV which is near the accuracy of the theoretical models and by increasing the basis space the convergence time increases dramatically, so we use the optimum basis space which is suitable for the present calculations. Thus $N_F$=$N_B$ $\geq$12 is enough for the convergence of the system which is shown in Figure 1.

To study the convergence of solutions in both RMF (NL3) and SHF (Sly4) formalisms, we have calculated the binding energy and corresponding quadrupole moment with different initial guess for the quadrupole moments. It is found that the calculated quadrupole deformation parameter $\beta_2$ is independent of the initial guess value of deformation $\beta_0$. Both the formalisms give almost similar results except spherical solution obtained with an initial deformation $\beta_0 = 0.03$. Due to this suspicious behavior of the SHF(SLy4) result at the spherical solution, we ignore it for further analysis. We perform the free calculation for $^{82,100,102,104}Zr$ isotopes and calculated results are given in Table 2. It is to be noted that from the potential energy surface curve as well as from the analysis of basis deformation, we get a spherical solution for lighter isotopes of Zr, such as $^{82-92}Zr$. However, the zero deformation does not stable for heavier masses of Zr upto A = 106. Again the appearence of zero solution get stabilize with increase mass number (see PES curve).

## 4. Calculations and Results

We used the non-constraint calculation in both the RMF and SHF formalisms. For this, first we put some initial guess value of basis deformation parameter and

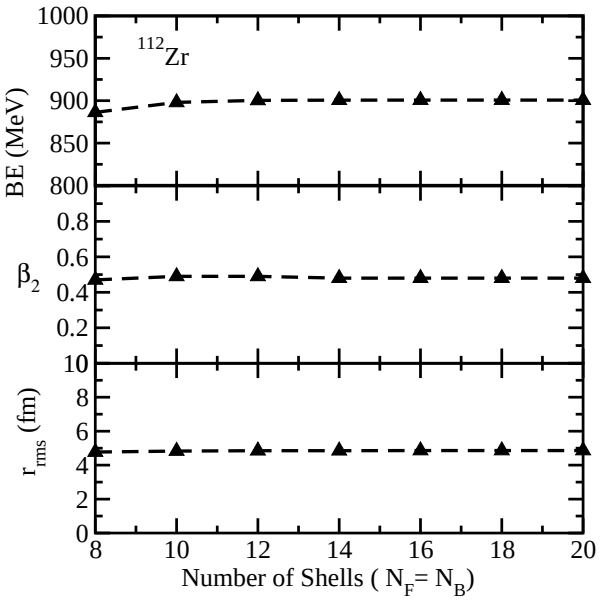


Fig. 1. (color online) The binding energy (BE), root mean square matter radius ($r_{rms}$) and quadrupole deformation parameter ($\beta_2$) with the harmonic oscillator basis.

let the system goes to find out the minimum energy state in local region corresponding to the initial guess i.e. $\beta_0$. We put the three guess values for each nucleus ($\beta_0 = 0.001, \pm 0.3$). In this case, final state (shape) of the nucleus may be different from the initial guess $\beta_0$ parameter. Both the SHF and RMF formalisms predict very good binding energy, root mean square (rms) radius and quadrupole deformation parameter $\beta_2$, not only for nuclei in stability line, but also for drip-lines nuclei. In this work, we have analyzed the structure of proton and neutron-rich Zr nuclei and studied two important phenomena such as (i) shape co-existence and (ii) parity doublet for some specific Zr isotopes. For this, we obtain matter radius $r_m$, quadrupole deformation parameter $\beta_2$ and ground state binding energy from proton to neutron drip-lines. The calculated results are given in Table 1 and the shape co-existence and parity doublets are shown in Figs. 3 to 6.

### 4.1. *Potential Energy Surface (PES)*

In our considered Zr isotopes, many nuclei are deformed in their ground state and for calculating the ground state properties one should include the deformation into the formalism. It may possible that some nuclei have almost same energy with

different shape configurations (spherical, prolate or oblate), this type of states are known as shape coexistence. To get the solution with different deformations one should perform the constraint calculation as a function of quadrupole deformation parameter with various constraint binding energy ($BE^c$). For constraint calculation, we minimized $< H^{'} >$ instead of $< H >$ which are related to each other by the following relation:[32–36]

$$H^{'} = H - \lambda Q, \qquad with \qquad Q = r^2 Y_{20}(\theta, \phi), \tag{19}$$

where, $\lambda$ is the Lagrange multiplier which is fixed by the constraint $< Q >_\lambda = Q_0$. We have done the constraint calculation for Zr isotopes for both the parameter sets (NL3 and SLy4) and obtained results are shown in Figure 2. We get almost similar results in both the formalisms. For example, the three minima of $^{110}Zr$ are located at $\beta_2$ = -0.217, 0.0 and 0.398 respectively. Similar situation can be found for $^{108,112}Zr$ nuclei. The ground-state potential energy surfaces allow us to determine the equilibrium shapes (the lowest minimum). It is worthy to mention here that the minima near zero is not well developed, but may be considered as an isomeric state.

The $\gamma-$soft configuration[37] is (energy almost constant for a large range of deformation) obtained in both models which clearly noticed in Fig. 2. For example, $^{84}$Zr isotopes have $\gamma-$soft surface near the $\beta_2$ ≈-0.2 to 0.5 deformation in RMF (NL3) model and $^{98}$Zr also followed the same trends in SHF(SLy4) formalism. In these cases, a triaxial calculation is most welcome to get a detail account on the potential energy surfaces. The free and constraint solution are giving the similar results for the ground state energy and shape configuration.

### 4.2. *Binding energy and shape co-existence*

The nuclear binding energy (BE) is a physical quantity, which is precisely measured experimentally and is responsible for nuclear stability and structure of nuclei. The maximum binding energy corresponds to the ground state and all other solutions are intrinsic excited states of a nucleus. These are not necessarily the lowest excitations, there could be rotational excitations below their first excited state, which is beyond the scope of our present calculations for further analysis. The BE for Zr isotopes obtained by SHF(SLy4) and RMF(NL3) calculations are depicted in Table 1 and the results compare with experimental data,[38–40] wherever available. From the ground and excited intrinsic states binding energies, we have measured their difference $\triangle BE = BE(gs) - BE(es)$ and examined the shape co-existence phenomena. When we find a small value of $\triangle BE$, then we termed it as a case of shape co-existence (degenerate solutions with different quadrupole deformations). The shape co-existence means, there is a maximum possibility of the nucleus, find in either shapes.

The binding energy difference between the ground and first and second intrinsic excited states are shown in Fig. 3 for Zr isotopes. The solid line is the zero reference

Table 1. The binding energy BE (MeV), root mean square radii (fm), quadrupole deformation parameter $\beta_2$ for Zr isotopes. The experimental results[38–40] are given for comparison.

| | RMF (NL3) | | | | | | SHF (SLy4) | | | | | | Expt. | | |
|---|---|---|---|---|---|---|---|---|---|---|---|---|---|---|---|
| Nucleus | $r_{ch}$ | $r_n$ | $r_p$ | $r_{rms}$ | BE | $\beta_2$ | $r_{ch}$ | $r_n$ | $r_p$ | $r_{rms}$ | BE | $\beta_2$ | $r_{ch}$ | $\beta_2$ | BE |
| | 4.282 | 4.123 | 4.207 | 4.165 | 664.5 | -0.172 | 4.276 | 4.125 | 4.201 | 4.163 | 665.9 | -0.154 | | | |
| $^{80}$Zr | 4.274 | 4.112 | 4.198 | 4.155 | 665.9 | 0.000 | 4.262 | 4.108 | 4.186 | 4.147 | 669.2 | 0.000 | | | 669.9 |
| | 4.362 | 4.207 | 4.288 | 4.248 | 665.1 | 0.480 | 4.393 | 4.243 | 4.319 | 4.281 | 665.3 | 0.5001 | | | |
| | 4.284 | 4.173 | 4.209 | 4.191 | 690.9 | -0.191 | 4.284 | 4.163 | 4.208 | 4.185 | 691.8 | -0.146 | | | |
| $^{82}$Zr | 4.272 | 4.158 | 4.197 | 4.177 | 691.7 | 0.000 | 4.269 | 4.151 | 4.193 | 4.172 | 694.4 | 0.000 | | 0.367 | 694.5 |
| | 4.371 | 4.262 | 4.297 | 4.279 | 689.6 | 0.480 | 4.372 | 4.248 | 4.298 | 4.272 | 690.4 | 0.430 | | | |
| | 4.324 | 4.453 | 4.249 | 4.367 | 809.8 | -0.148 | 4.348 | 4.397 | 4.274 | 4.345 | 813.5 | -0.133 | | | |
| $^{94}$Zr | | | | | | | 4.327 | 4.385 | 4.253 | 4.329 | 814.1 | 0.000 | 4.332 | 0.094 | 814.7 |
| | 4.326 | 4.452 | 4.251 | 4.368 | 809.4 | 0.163 | 4.383 | 4.421 | 4.309 | 4.373 | 813.5 | 0.242 | | | |
| | 4.355 | 4.521 | 4.281 | 4.423 | 822.9 | -0.191 | 4.371 | 4.449 | 4.297 | 4.386 | 825.8 | -0.152 | | | |
| $^{96}$Zr | 4.368 | 4.520 | 4.294 | 4.427 | 823.2 | 0.240 | 4.446 | 4.499 | 4.374 | 4.447 | 824.2 | 0.345 | 4.351 | 0.08 | 829.0 |
| | 4.381 | 4.585 | 4.307 | 4.473 | 835.4 | -0.215 | 4.403 | 4.506 | 4.330 | 4.435 | 838.4 | -0.196 | | | |
| $^{98}$Zr | 4.501 | 4.676 | 4.429 | 4.577 | 836.0 | 0.497 | 4.502 | 4.579 | 4.431 | 4.519 | 836.9 | 0.430 | 4.401 | | 840.9 |
| | 4.400 | 4.639 | 4.327 | 4.517 | 846.9 | -0.217 | 4.427 | 4.555 | 4.354 | 4.476 | 849.4 | -0.210 | | | |
| $^{100}$Zr | 4.487 | 4.690 | 4.415 | 4.582 | 847.7 | 0.445 | 4.512 | 4.612 | 4.441 | 4.545 | 849.7 | 0.421 | 4.49 | 0.355 | 852.2 |
| | 4.416 | 4.687 | 4.343 | 4.555 | 858.0 | -0.206 | 4.449 | 4.599 | 4.376 | 4.513 | 859.7 | -0.215 | | | |
| $^{102}$Zr | 4.496 | 4.732 | 4.424 | 4.614 | 858.3 | 0.430 | 4.536 | 4.654 | 4.465 | 4.581 | 860.5 | 0.429 | 4.53 | 0.427 | 863.6 |
| | 4.436 | 4.735 | 4.363 | 4.595 | 868.7 | -0.207 | 4.469 | 4.64 | 4.397 | 4.548 | 869.6 | -0.219 | | | |
| $^{104}$Zr | 4.404 | 4.715 | 4.331 | 4.571 | 865.2 | 0.000 | 4.426 | 4.617 | 4.353 | 4.517 | 866.8 | 0.000 | | | 873.8 |
| | 4.512 | 4.780 | 4.441 | 4.652 | 867.9 | 0.424 | 4.557 | 4.696 | 4.486 | 4.617 | 870.2 | 0.430 | | | |
| | 4.461 | 4.783 | 4.389 | 4.639 | 878.5 | -0.226 | 4.49 | 4.68 | 4.418 | 4.583 | 879.2 | -0.223 | | | |
| $^{106}$Zr | 4.422 | 4.764 | 4.349 | 4.612 | 876.0 | 0.000 | 4.444 | 4.658 | 4.372 | 4.552 | 876.1 | 0.000 | | | 883.2 |
| | 4.534 | 4.825 | 4.463 | 4.691 | 877.6 | 0.420 | 4.574 | 4.734 | 4.503 | 4.648 | 879.3 | 0.421 | | | |
| | 4.483 | 4.829 | 4.411 | 4.679 | 886.8 | -0.232 | 4.509 | 4.717 | 4.437 | 4.616 | 887.5 | -0.226 | | | |
| $^{108}$Zr | 4.439 | 4.816 | 4.366 | 4.654 | 886.5 | 0.000 | 4.463 | 4.697 | 4.391 | 4.586 | 885.2 | 0.000 | | | 891.7 |
| | 4.556 | 4.873 | 4.485 | 4.733 | 886.8 | 0.420 | 4.592 | 4.769 | 4.522 | 4.679 | 887.6 | 0.414 | | | |
| | 4.487 | 4.865 | 4.415 | 4.707 | 894.3 | -0.190 | 4.521 | 4.749 | 4.45 | 4.642 | 894.3 | -0.210 | | | |
| $^{110}$Zr | 4.454 | 4.864 | 4.381 | 4.964 | 896.2 | 0.000 | 4.48 | 4.733 | 4.408 | 4.617 | 893.9 | 0.000 | | | 899.5 |
| | 4.595 | 4.955 | 4.525 | 4.803 | 893.9 | 0.473 | 4.621 | 4.824 | 4.551 | 4.727 | 894.4 | 0.437 | | | |
| | 4.500 | 4.904 | 4.429 | 4.740 | 901.9 | -0.171 | 4.53 | 4.775 | 4.459 | 4.664 | 901.1 | -0.176 | | | |
| $^{112}$Zr | 4.469 | 4.903 | 4.397 | 4.729 | 902.7 | 0.000 | 4.496 | 4.765 | 4.424 | 4.646 | 901.1 | 0.000 | | | 906.5 |
| | 4.620 | 5.001 | 4.550 | 4.845 | 900.5 | 0.480 | 4.645 | 4.874 | 4.576 | 4.77 | 900.9 | 0.453 | | | |

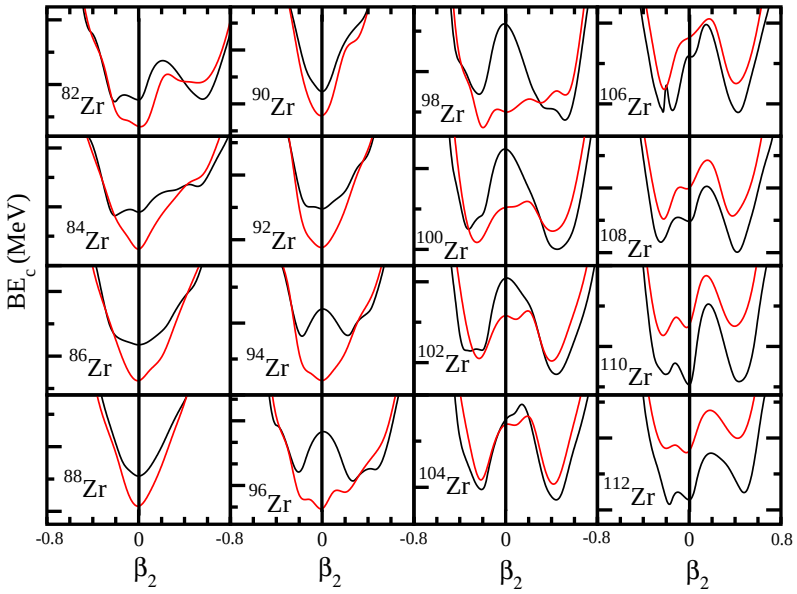


Fig. 2. (color online) The potential energy surface for the Zr isotopes for NL3 (black line) and SLy4 (red line) force parameter.

label, which marks the shape co-existence line. The points which are on the line are designated as perfectly shape co-existence nuclei. The shape co-existence in $A = 80$ mass region of nuclei using RMF formalism is reported in Refs.[3,28,41] Here, it has shown that the neutron deficient nuclei in this mass region possess spherical and largedeformed structures. In the present work, we would like to show that not only the neutron-deficient Zr isotopes have shape co-existence, but also other normal and neutron-rich Zr isotopes have low-lying largedeformed configuration including the normal/spherical shape. Some times it so happens that the largedeformed solution becomes the ground state ($^{98}Zr$, $\beta_2$=0.497 in RMF ) as shown in the Table 1. The nuclei with shape co-existence shows the transition between the spherical to oblate to prolate due to minimum energy barrier between the shape co-existence states. There are many isotopes ($^{96,98,100,102,108}$Zr), which have $\Delta BE \leq 1$ MeV for both cases like $1^{st}$ and $2^{nd}$ intrinsic excited states. These type of shape co-existence called triple shape co-existence.[8] If we see the $\Delta BE$ for $^{108}$Zr in Figure 3, its excited state has almost same energy with its ground state, leading to the phenomenon of shape co-existence. These type of nuclei show the shape co-existence in their excited state and performed the shape change/ fluctuation in application of a small

Table 2. The binding energy BE (MeV), quadrupole deformation parameter $\beta_2$ and basis deformation parameter $\beta_0$ for Zr isotopes.

| | RMF (NL3) | | SHF (SLy4) | | | | RMF (NL3) | | SHF (SLy4) | | |
|---|---|---|---|---|---|---|---|---|---|---|---|
| Nucleus | BE | $\beta_2$ | BE | $\beta_2$ | $\beta_0$ | Nucleus | BE | $\beta_2$ | BE | $\beta_2$ | $\beta_0$ |
| | 691.0 | -0.194 | 691.8 | -0.182 | -0.6 | | 858.1 | -0.208 | 859.7 | -0.216 | -0.6 |
| | 691.0 | -0.192 | 691.8 | -0.178 | -0.5 | | 858.1 | -0.206 | 859.7 | -0.216 | -0.5 |
| | 690.9 | -0.191 | 691.8 | -0.146 | -0.4 | | 858.0 | -0.205 | 859.7 | -0.215 | -0.4 |
| | 690.9 | -0.191 | 691.8 | -0.164 | -0.3 | | 858.0 | -0.206 | 859.7 | -0.215 | -0.3 |
| | 690.8 | -0.190 | 692.2 | -0.117 | -0.2 | | 858.0 | -0.206 | 859.7 | -0.215 | -0.2 |
| | 691.7 | 0.000 | 692.5 | -0.103 | -0.1 | | 858.0 | -0.207 | 859.7 | -0.215 | -0.1 |
| $^{82}Zr$ | 691.7 | 0.000 | 694.4 | 0.000 | 0.03 | $^{102}Zr$ | 858.2 | 0.419 | 857.3 | 0.000 | 0.0.3 |
| | 691.7 | 0.000 | 690.0 | 0.461 | 0.1 | | 858.3 | 0.426 | 860.5 | 0.429 | 0.1 |
| | 691.7 | 0.000 | 690.0 | 0.477 | 0.2 | | 858.3 | 0.429 | 860.5 | 0.428 | 0.2 |
| | 689.4 | 0.493 | 690.0 | 0.493 | 0.3 | | 858.2 | 0.429 | 860.6 | 0.428 | 0.3 |
| | 689.4 | 0.481 | 690.0 | 0.496 | 0.4 | | 858.2 | 0.429 | 860.6 | 0.428 | 0.4 |
| | 689.4 | 0.473 | 690.0 | 0.484 | 0.5 | | 858.3 | 0.430 | 860.5 | 0.429 | 0.5 |
| | 689.6 | 0.480 | 690.4 | 0.430 | 0.6 | | 858.1 | 0.428 | 860.5 | 0.429 | 0.6 |
| | | | | | | | | | | | |
| | 846.9 | -0.218 | 849.4 | -0.212 | -0.6 | | 868.7 | -0.208 | 869.6 | -0.220 | -0.6 |
| | 846.9 | -0.217 | 849.4 | -0.211 | -0.5 | | 868.7 | -0.206 | 869.6 | -0.219 | -0.5 |
| | 846.9 | -0.216 | 849.4 | -0.211 | -0.4 | | 868.7 | -0.206 | 869.6 | -0.219 | -0.4 |
| | 846.9 | -0.217 | 849.4 | -0.210 | -0.3 | | 868.7 | -0.207 | 869.6 | -0.219 | -0.3 |
| | 846.8 | -0.218 | 849.4 | -0.210 | -0.2 | | 868.6 | -0.207 | 869.7 | -0.219 | -0.2 |
| | 846.8 | -0.218 | 849.5 | -0.210 | -0.1 | | 868.6 | -0.208 | 869.7 | -0.219 | -0.1 |
| $^{100}Zr$ | 847.6 | 0.423 | 847.5 | 0.000 | 0.03 | $^{104}Zr$ | 865.2 | 0.000 | 866.8 | 0.000 | 0.03 |
| | 847.7 | 0.440 | 849.7 | 0.423 | 0.1 | | 865.1 | 0.035 | 870.3 | 0.430 | 0.1 |
| | 847.7 | 0.449 | 849.7 | 0.422 | 0.2 | | 868.0 | 0.424 | 870.3 | 0.430 | 0.2 |
| | 847.7 | 0.445 | 849.7 | 0.421 | 0.3 | | 868.0 | 0.424 | 870.3 | 0.430 | 0.3 |
| | 847.6 | 0.440 | 849.7 | 0.422 | 0.4 | | 867.9 | 0.424 | 870.3 | 0.430 | 0.4 |
| | 847.6 | 0.436 | 849.7 | 0.423 | 0.5 | | 867.9 | 0.423 | 870.3 | 0.430 | 0.5 |
| | 847.6 | 0.433 | 849.6 | 0.422 | 0.6 | | 867.9 | 0.424 | 870.2 | 0.430 | 0.6 |

energy ($\leq 1$ MeV). The shape co-existence is very important in the reaction study, because surface density distribution plays a crucial role in the cross-section and it will change by applying small perturbation in energy. Some isotopes of Zr are predicted to be triaxial ($\gamma \neq 0$)[42] in shape, which is one more degree of freedom in shape orientation. The study of phenomenon is beyond the scope of this work, as we have used the axially symmetric formalism for the deformed nuclei.

Analyzing Fig. 3 and the binding energy results of Table 1, it is clear that the prediction of RMF(NL3) and SHF(SLy4) are almost similar. Again, comparing the results with experimental data, the SLy4 parameter set reproduce the data similar

Table 3. The pairing gap, effective strenth and pairing energy for Zr isotopes.

| | RMF (NL3) | | | SHF (SLy4) | | | | |
|---|---|---|---|---|---|---|---|---|
| Nucleus | $\triangle_n$ | $\triangle_p$ | $E_{pair}$ | $G_n$ | $G_p$ | $\triangle_n$ | $\triangle_p$ | $E_{pair}$ |
| $^{80}Zr$ | 1.673 | 1.673 | 18.995 | -0.162 | -0.158 | 0.158 | 0.143 | 4.578 |
| $^{82}Zr$ | 1.633 | 1.669 | 19.078 | -0.149 | -0.157 | 0.217 | 0.142 | 5.911 |
| $^{94}Zr$ | 1.242 | 1.422 | 15.188 | -0.126 | -0.145 | 0.169 | 0.124 | 4.485 |
| $^{96}Zr$ | 1.170 | 1.361 | 13.882 | -0.125 | -0.144 | 0.183 | 0.118 | 4.889 |
| $^{98}Zr$ | 1.100 | 1.300 | 11.999 | -0.125 | -0.141 | 0.194 | 0.135 | 5.44 |
| $^{100}Zr$ | 1.031 | 1.238 | 11.411 | -0.121 | -0.140 | 0.222 | 0.133 | 6.156 |
| $^{102}Zr$ | 0.966 | 1.176 | 10.767 | -0.118 | -0.138 | 0.251 | 0.131 | 6.695 |
| $^{104}Zr$ | 0.903 | 1.115 | 9.886 | -0.116 | -0.134 | 0.163 | 0.103 | 4.183 |
| $^{106}Zr$ | 0.844 | 1.056 | 8.840 | -0.114 | -0.133 | 0.158 | 0.095 | 3.948 |
| $^{108}Zr$ | 0.787 | 0.999 | 7.741 | -0.112 | -0.132 | 0.139 | 0.091 | 3.517 |
| $^{110}Zr$ | 0.735 | 0.944 | 6.971 | -0.109 | -0.133 | 0.143 | 0.084 | 3.468 |
| $^{112}Zr$ | 0.685 | 0.892 | 6.959 | -0.106 | -0.132 | 0.124 | 0.082 | 3.058 |

or even better than NL3 set of the RMF formalism. In general, both the SHF and RMF have tremendous predictive power upto a great extend of accuracy and can be used the results to most part of the mass Table.

### 4.3. *Evolution of single particle energy with deformation*

In this section, we have calculated the single particle energy of some selected Nilsson orbits with the different values of deformation parameter $\beta_2$ by the constraint calculation. The obtained results are given in Figure 4, where positive parity orbits shown by dotted and negative parity by solid lines for $^{100}$Zr isotope. The single particle energy for neutron is given in Figure 4(a) and proton single particle energy in Figure 4(b). The lower level like $\frac{1}{2}^+[000]$ is very less affected by the variation of the deformation in both neutron and proton cases as shown in Figure 4(a,b). But as increase the energy of the levels, variation of single particle energy is also increases with the deformation parameter as shown in Figure. We have plotted similar curve for $\frac{3}{2}^{\pm}$ orbits for the same nucleus $^{100}$Zr and obtained results are given in Figure 4(c,d) for neutron and proton, respectively. The evolution of single particle energy levels with deformation parameters followed similar nature of $\frac{1}{2}^{\pm}$ orbits. We repeated the calculation in non-relativistic SHF model also and obtained almost similar trend of levels, so we are not presenting the SHF results for the single particle energy evolution with deformation in the present manuscript. The single particle energies are evolved with the deformation parameter and opposite parity orbits are come closer with deformation. A detail study is done in next section, where we will discuss about the parity doublets in the orbits at large deformation.

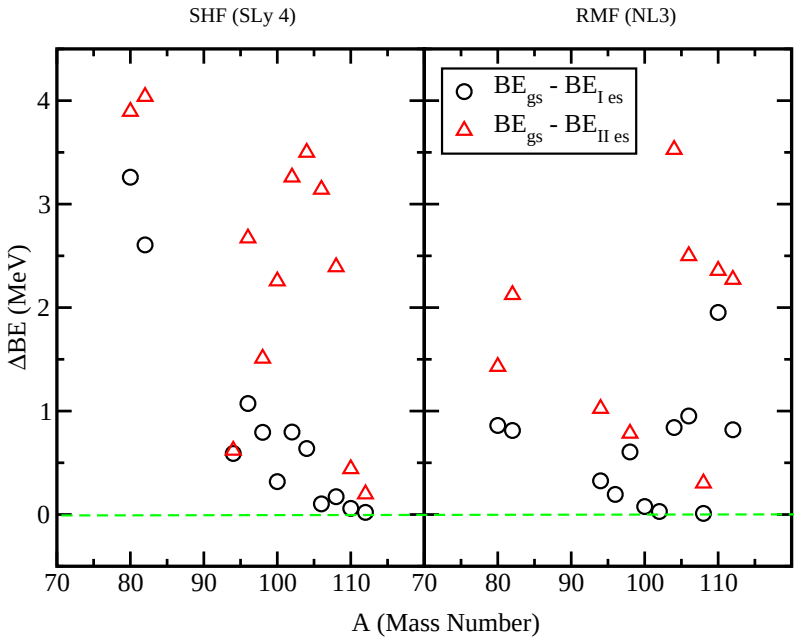


Fig. 3. (color online) The ground state binding energy difference from first and second intrinsic excited states for Zr isotopes. The zero reference point shown by the dashed horizontal line.

### 4.4. *Largedeformed configuration and parity doublet*

The parity doublet is an interesting configuration for the largedeformed state of a nucleus. Recently, it is reported by Singh et al.[1] that, there exist a parity doublet in the largedeformed configuration for light mass nuclei. In the present calculations, we have extended the investigation to relatively heavier mass region of the periodic chart. In this case, we focused our study for Zr isotopes, where shape co-existence is an usual phenomenon. In most of the cases of Zr isotopes, we get a spherical or a normal deformed solution along with a largedeformed state both in the RMF(NL3) and SHF(SLy4) calculations. The evolution of single particle energy with deformation parameter $\beta_2$ for some selected nuclei are depicted in Figs. 5 and 6. The parity doublets are marked by their asymptotic quantum number [N, $n_z$, $\Lambda$], where N is principle quantum number, $n_z$ is number of nodes of the wave function in the $z-$direction (the number of times the radial wave function crosses zero). Larger $n_z$ values corresponds to wave function more extended in the $z-$direction which means lower energy orbits, $\Lambda$ is the projection of the orbital angular momentum on to the $z-$axis. Similar to the case of light mass nuclei,[1] in case of Zr isotopes also, the deformation-driving $\Omega^{\pi} = \frac{1}{2}^{-}$ orbits come down in energy in largedeformed solu-

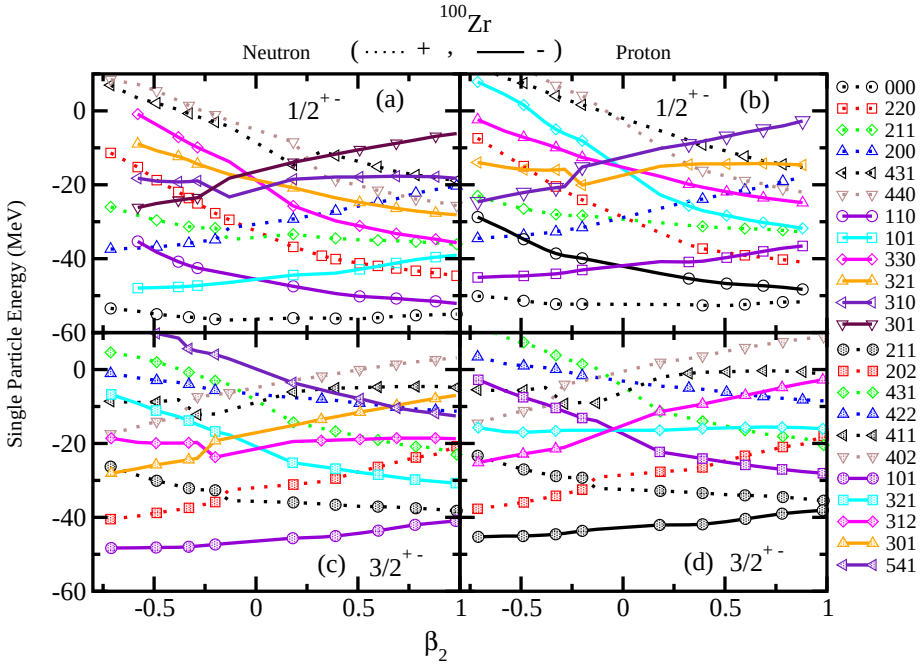


Fig. 4. (color online) Some selected single particle (s.p.) energy level evolution with deformation parameter $\beta_2$ for relativistic model by using NL3 parameter set. (a) 1/2+- s.p. levels for the neutron, (b) 1/2+- levels for proton, (c) 3/2+- s.p. levels for neutron, and (d) 3/2+- s.p. levels for proton. The positive parity (+) level is given by dotted line and negative parity levels (-) level is given by solid line.

tions from the shell above, in contrast to the normal deformed solutions. For each nucleus, we have compared the normal/spherical deformed and the largedeformed configurations single particle energy orbits and analyzed the parity doublets states and some of them are given in this work. The occurrence of approximate $\frac{1}{2}^+$, $\frac{1}{2}^-$ parity doublets (degeneracy of $\Omega^\pi = \frac{1}{2}^+$, $\frac{1}{2}^-$ states) for the largedeformed solutions are clearly seen in Figs. 5 and 6, where excited largedeformed configurations for $^{80}$Zr and $^{100}$Zr are given. As shown in Figure 5, the energy level for spherical shape for opposite parity are well separated from each other, but becomes closer with deformation which shows the parity doublets in the system. For example, in case of $^{80}$Zr, if we plot the single particle energy level for neutron, then the energy levels $[310]\frac{1}{2}^-$ and $[440]\frac{1}{2}^+$ are far from each other ($\sim$ 18.28 MeV in RMF), but becomes almost degenerate ($\sim$ 1.28 MeV) at largedeformation ($\beta_2 = 0.480$). Same behavior we found in the single particle energy orbits $[440]\frac{1}{2}^+$ and $[310]\frac{1}{2}^-$ of proton intrinsic single particle energy distribution, i.e. in normal deformation, these two levels are separated from each other by 16.8 MeV, but in largedeformed case ($\beta_2$=0.480),

it becomes closer ($\sim$ 0.5 MeV). Qualitatively, the same behavior appears in the SHF(SLy4) results also (left panel of the Figure). In Figure 6, for $^{100}$Zr we have given the largedeformed orbits for prolate and oblate cases both for RMF(NL3) and SHF(SLy4) models. Here also, we are getting the parity doublet in oblate and prolate shapes, which implies that parity doublets are driving by the deformation and it will occur at the large deformation. Some parity doublet orbits are shown by Nilsson representation [N, $n_z$, $\Lambda$] in Figure 6. If we put close inspection on Figure 6, then in the oblate level of neutron, we get several parity doublets like ([411] [330]), ([440] [510]) and for proton ([330] [411]). For prolate case, the neutron parity doublet orbits ([530] [400]), ([550] [420]), ([301] [431]), ([310] [440]) etc, similarly for the proton case.

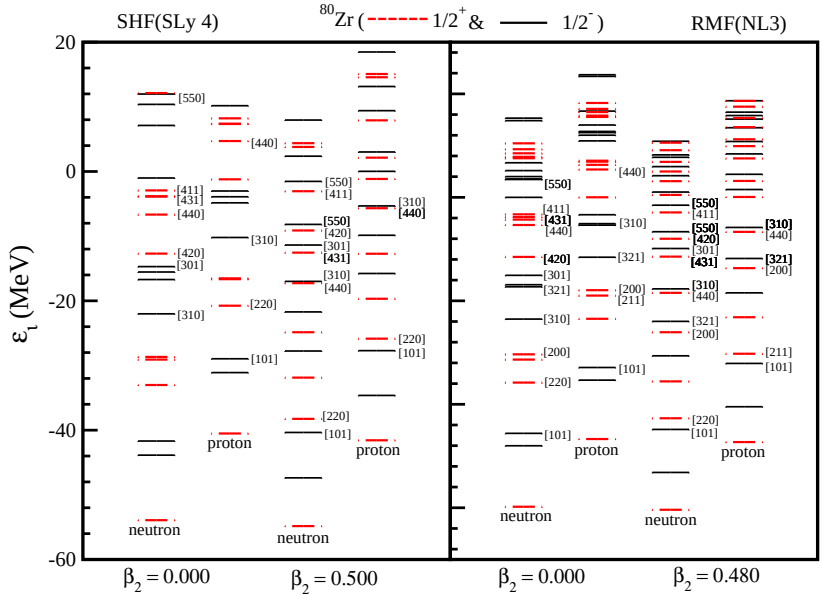


Fig. 5. (color online) Single-particle levels for $^{80}$Zr in normal and largedeformed states. The single-particle levels are denoted by the Nilsson indices [N, $n_z$, $\Lambda$]$\Omega^{\pi}$.

## 5. Summary and Conclusions

We calculate the ground and low-lying excited state properties, like binding energy and quadrupole deformation parameter $\beta_2$ using RMF(NL3) and SHF(SLy4) formalisms for Zr isotopes near the drip-line regions. In general both the RMF and

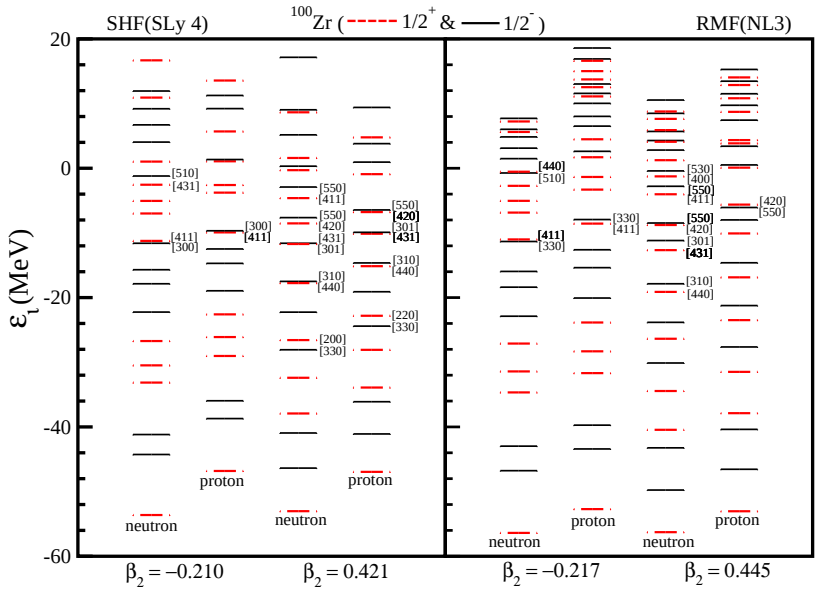


Fig. 6. (color online) Single-particle levels for $^{100}$Zr isotopes in oblate and largedeformed states.

SHF predict very good results throughout the isotropic chain. We are getting the double and triple shape co-existence from our analysis in some Zr isotopes, which is consistent with the earlier data. The present prediction of parity doublet may be a challenge for the experimentalist to look for such configuration states. In general, we find large deformed solutions for the neutron-drip nuclei, which agree with the experimental measurements. In the calculations, a large number of low-lying intrinsic largedeformed excited states are predicted in many of the isotopes, which shows the parity doublet near the Fermi levels. The parity doublet levels are nearly degenerated in excited states which can make the two different parity band by transition of two particles from reference frame to these degenerate opposite parity levels. It may be solved the problem of existence of the twin bands and quantization of alignments of shapes. This analysis will help us to understand the intrinsic excited states of the Zr and other similar isotopes. In this respect, some more calculations are required to build a general idea about the omega parity doublets.

## References

1. S. K. Singh, C. R. Praharaj and S. K. Patra, Cen. Eur. J. Phys. **12**, (2014) 42.
2. K. Sugawara-Tanabe and A. Arima, Phys. Lett. B **317**, (1993) 1.

3. J. P. Maharana, Y. K. Gambhir, J. A. Sheikh and P. Ring, Phys. Rev. C **46**, (1992) R1163.
4. S. K. Patra and C. R. Praharaj, Phys. Rev. C **47**, (1993) 2978.
5. F. Sarazin et al., Phys. Rev. Lett. **84**, (2000) 5062.
6. J. L. Egido, L. M. Robledo and R. R. Rodriguez-Guzman, Phys. Rev. Lett. **93**, (2004) 282502.
7. S. K. Singh, M. Ikram and S. K. Patra, Int. J. Mod. Phys. E **22**, (2013) 1350001.
8. A. Petrovici, Phys. Rev. C **85**, (2012) 034337.
9. M. V. Stoitsov, J. Dobaczewski, W. Nazarewicz, S. Pittel and D. J. Dean, Phys. Rev. C **68**, (2003) 054312.
10. E. Chabanat, P. Bonche, P. Haensel, J. Meyer and R. Schaeffer, Nucl. Phys. A **635**, (1998) 231.
11. M.V. Stoitsov, J. Dobaczewski, W. Nazarewicz and P. Ring Computer Physics Communications **167**, (2005) 43.
12. H. J. Lipkin, Ann. of Phys. **9**, ( 1960) 272.
13. H. Flocard and N. Onishi, Ann. Phys. (NY) **254**, (1997) 275.
14. P. Ring, P. Schuck, The Nuclear Many-Body Problem, Springer-Verlag, Berlin, 1980.
15. P. Ring, Y. K. Gambhir and G. A. Lalazissis, Computer Physics Communications **105**, (1997) 77.
16. M. Bender,P.-H. Heenen and P. G. Reinhard, Rev. Mod. Phys. **75**, (2003) 121.
17. E. Perlińska, S.G. Rohoziński, J. Dobaczewski and W. Nazarewicz, Phys. Rev. C **69**, (2004) 014316.
18. K. Bennaceur, J. Dobaczewski, Computer Physics Communications **168**, (2005) 96.
19. Y. K. Gambhir, P. Ring and A. Thimet, Ann. Phys. (NY) **198**, (1990) 132.
20. S. K. Patra and C. R. Praharaj, Phys. Rev. C **44**, (1991) 2552.
21. J. D. Walecka, Ann. Phys. (NY) **83**, (1974) 491.
22. B. D. Serot and J. D. Walecka, Adv. Nucl. Phys. **16**, (1986) 1.
23. C. J. Horowitz and B. D. Serot, Nucl.Phys. A **368**, (1981) 503.
24. J. Boguta and A. R. Bodmer, Nucl. Phys. A **292**, (1977) 413.
25. C. E. Price and G. E. Walker, Phys. Rev. C **36**, (1987) 354.
26. G. A. Lalazissis, J. König and P. Ring, Phys. Rev. C **55**, (1997) 1.
27. D. G. Madland and J. R. Nix, Nucl. Phys. A **476**, (1981) 1.
28. S. K. Patra, Phys. Rev. C **48**, (1993) 1449.
29. M. A. Preston and R. K. Bhaduri, *Structure of Nucleus, Addison-Wesley Publishing Company*, Ch. 8, page 309 (1982).
30. J. Decharg and D. Gogny, Phys. Rev. C **21**, (1980) 1568.
31. S. Karatzikos, A. V. Afanasjev, G. A. Lalazissis, P. Ring, Phys. Lett. B **689**, (2010) 72.
32. S. K. Patra, F. H. Bhat, R. N. Panda, P. Arumugam and R. K. Gupta, Phys. Rev. C **79**, (2009) 044303.
33. H. Flocard, P. Quentin and D. Vautherin, Phys. Lett. B **46**, (1973) 304.
34. W. Koepf and P. Ring, Phys. Lett. B **212**, (1988) 397.
35. J. Fink, V. Blum, P.-G. Reinhard, J. A. Maruhn and W. Greiner, Phys. Lett. B **218**, (1989) 277.
36. D. Hirata, H. Toki, I. Tanihata and P. Ring, Phys. Lett. B **314**, (1993) 168.
37. J. Dobaczewski, S. G. Rohozifiski and J. Srebrny, Z. Physik A **282**, (1977) 203.
38. S. Raman, C. W. Jr. Nestor and P. Tikkanen, At. Data and Nucl. Data Tables **78**, (2001) 1.
39. M. Wang, G. Audi, A. H. Wapstra, F. G. Kondev, M. Mac-Cormick, X. Xu and B. Pfeiffer, Chin. Phys. C **36**, (2012) 1603.

40. I. Angeli and K. P. Marinova, At. Data and Nucl. Data Tables **99**, (2013) 69.
41. A. Chakraborty et al., Phys. Rev. Lett. **110**, (2013) 022504.
42. Tomás R. Rodríguezguez and J. Luis Egido, arXiv:1109.6511v1